

The Impact of Telecom Fraud Activity in Northern Myanmar on the China–Myanmar Border Region

Xinyuan Lyu*

April 2025

Abstract

This study examines the economic impact of telecom fraud activities in northern Myanmar on adjacent China-Myanmar border regions. Leveraging grid-level nighttime light (NTL) intensity data and city-level migration indices, the research identifies dual impacts: a localized short-term economic stimulus near border crossings and broader negative reputational effects leading to reduced legitimate migration. Utilizing difference-in-differences, event-study models, and Synthetic Control Methods, the analysis provides empirical evidence highlighting the complexity of cross-border illicit activities' influence on regional economies.

Keywords: Telecom Fraud, Illicit Economies, Myanmar-China Border, Migration

JEL Codes: O17, R12, F22, K42

*Department of Economics, Duke University. Email: xinyuan.lyu@duke.edu

1 Introduction

Cross-border illicit activities, such as telecom fraud, represent an increasingly severe global concern, posing complex challenges for both security and economic development, particularly in border regions with weak governance structures. Recently, northern Myanmar has emerged as a significant hub for large-scale telecommunications fraud operations, primarily targeting victims in neighboring China and other countries. These activities have not only involved organized criminal networks but also attracted a considerable influx of Chinese nationals voluntarily or involuntarily, thereby intensifying local and cross-border socio-economic dynamics.

Over the past few years, these scam compounds have expanded into a large-scale industry. Chinese authorities have repeatedly described northern Myanmar and the surrounding Mekong region as one of the main overseas bases for telecom and online fraud targeting Chinese citizens, and report that joint law-enforcement operations have led to the arrest and repatriation of over 50,000 Chinese nationals suspected of involvement in such schemes since 2023.¹ According to the United Nations Office of the High Commissioner for Human Rights, hundreds of thousands of people have been trafficked into scam centres across Southeast Asia and forced into online criminality.² At the same time, major scam hubs in northern Myanmar lie along key sections of the China–Myanmar border that coincide with some of China’s most important overland trade corridors. This combination of mass victimization, large-scale illicit profits, and strategic geographic location means that telecom fraud is no longer merely a law-enforcement issue, but a central challenge for border governance and regional economic development.

This paper investigates the economic consequences of these burgeoning telecom fraud

¹Ministry of Public Security of China, “New results in the China–Myanmar joint crackdown on telecom and online fraud,” 23 April 2025. Available at: <https://www.mps.gov.cn/n2255079/n4876594/n5104076/n5104077/c10056402/content.html>.

²UN Office of the High Commissioner for Human Rights, “Hundreds of thousands trafficked to work for online scammers in Southeast Asia,” 29 August 2023. Available at: <https://www.ohchr.org/en/press-releases/2023/08/hundreds-thousands-trafficked-work-online-scammers-se-asia-says-un-report>.

activities starting in 2019 for the adjacent China-Myanmar border regions, examining both direct local economic impacts and broader indirect effects through population mobility patterns. Given the inherent challenges in directly observing illicit economic activities and measuring their precise economic impact, this study leverages satellite-based nighttime light (NTL) data and mobile phone-based migration indices as proxies for economic and human activity.

Specifically, this research addresses two interrelated hypotheses. First, it explores whether the substantial influx of people and associated illicit activities related to telecom fraud operations might stimulate short-term economic activity in border-adjacent areas. Second, it also investigates whether the growing presence of organized crime negatively impacts the broader region's reputation, thereby deterring legitimate economic activities such as tourism, investment, and general migration.

Therefore the empirical analysis proceeds in two main parts. First, grid-level nighttime light intensity data are used in a difference-in-differences and event-study framework to quantify localized economic impacts associated with proximity to border crossings. Second, the study utilizes city-level migration indices within a Synthetic Control framework to assess changes in population mobility patterns in Chinese border cities following the intensification of telecom fraud activities.

These developments have triggered an unprecedented wave of cross-border enforcement campaigns and public concern, yet there is still little systematic evidence on how the telecom-fraud boom has reshaped local economies and population mobility on the Chinese side of the border. Providing such evidence is urgent not only for evaluating past enforcement efforts, but also for designing future policies that jointly address security risks and the economic prospects of border communities.

This investigation makes two main contributions. First, it provides the first systematic analysis in the economics literature of the economic consequences of Myanmar-based telecom-fraud operations. By documenting both localized short-run stimulus effects and broader

reputational damages, the paper clarifies how illicit cross-border activities shape economic development in border regions. Second, the paper proposes a reusable empirical framework for studying telecom fraud in Myanmar and related topics, combining satellite-based night-time lights, mobile-phone-based migration indices, and quasi-experimental methods that can serve as a template for future work.

2 Related Literature

This study intersects with several branches of economic literature that examine the complex interplay between illicit activities, governance, migration, and local economic development, particularly in border regions.

Illicit Economies and Local Development A significant body of work investigates the impact of illicit economies, such as drug trafficking or organized crime, on local development outcomes. For instance, using a spatial regression discontinuity design in Mexico, Dell (2015) finds that the election of PAN mayors, who implemented aggressive anti-drug policies, led to significant increases in drug-related violence, as rival cartels vied for control in the power vacuums created. And studies on organized crime in developed countries, like Pinotti (2015), demonstrate that mafia presence in Italy significantly hampers firm productivity and aggregate economic performance by distorting markets and deterring investment. More recently, Melnikov et al. (2025) studies the emergence of gang-controlled territories in El Salvador and find that individuals living just within gang-controlled areas experience significantly worse material well-being, lower income, and lower educational attainment than nearby individuals just outside such areas.

Illicit Activities, Violence, and Migration Some recent empirical studies provide mixed evidence on whether violence leads to large-scale displacement. Basu and Pearlman (2017) analyze homicide-driven violence stemming from Mexico's drug war since 2006

and find only limited evidence that increased homicides caused internal or international out-migration at the municipal level, suggesting a muted migration response. Similarly, Aldeco Leo et al. (2024) finds that although homicide spikes reduce the likelihood of high-skilled individuals migrating into violent municipalities, most out-migration is localized within the same commuting zone. These findings suggest that while violence in illicit economies can influence migration patterns, the response is shaped by structural factors such as skill levels, migration costs, and local labor market conditions. However, illicit economies and criminal networks may also attract individuals who actively seek high-risk, high-reward opportunities. And this kind of selective in-migration remains largely underexplored in the literature.

Criminal Groups and Governance Recent literature has also explored the intricate relationships between criminal organizations and governance structures, highlighting scenarios where criminal groups effectively govern communities in place of, or alongside, formal state institutions. Uribe et al. (2022) utilizes comprehensive survey data across Latin America, identifying extensive prevalence of criminal governance affecting millions. Interestingly, they find criminal governance positively correlates with both perceived and actual state governance quality, challenging conventional views that weak states directly facilitate criminal rule. Similarly, Blattman et al. (2024) analyze gang rule dynamics in Medellín, Colombia, demonstrating that increased state presence can ironically bolster gang governance as gangs strategically govern to minimize state intervention threats. These studies emphasize the complex and often counterintuitive dynamics between state capacity and criminal governance.

Ethnic Armed Organisations and Myanmar Civil War In the context of the China–Myanmar border, ethnic armed organizations (EAOs) have historically maintained control over semi-autonomous territories, facilitating the growth of illicit activities such as drug trafficking, illegal resource extraction, and, more recently, telecom fraud. These EAOs have established complex political economies where illicit proceeds not only fund their operations but also

shape local power dynamics and governance structures (MacBeath, 2025). The entrenchment of these illicit economies has been further exacerbated by the 2021 military coup in Myanmar, which led to a significant weakening of central authority and allowed EAOs to expand their influence and economic activities (Peng, 2024).

This study aims to contribute to these literatures by providing empirical evidence on the specific economic consequences of the recent surge in telecom fraud operations situated in the complex governance landscape of the China-Myanmar border region.

3 Background

Telecom and online fraud based in northern Myanmar has recently emerged as a major form of organized criminal activity in border regions such as Kokang, Wa State, and Myawaddy. Large-scale scam operations in these areas primarily target victims in China and other countries using a variety of online schemes. A distinctive feature of this illicit industry is its reliance on a sizeable workforce that includes large numbers of Chinese nationals, many of whom are reportedly lured, trafficked, or coerced into participating. Chinese authorities describe northern Myanmar and the surrounding Mekong region as one of the main overseas bases for telecom and online fraud targeting Chinese citizens, and report that special joint operations since 2023 have led to the arrest and repatriation of over 53,000 Chinese nationals suspected of involvement in such schemes.³ At the regional level, the United Nations Office of the High Commissioner for Human Rights estimates that *hundreds of thousands* of people have been trafficked into scam centres across Southeast Asia and forced into online criminality.⁴

³Ministry of Public Security of China, “New results in the China–Myanmar joint crackdown on telecom and online fraud,” 23 April 2025, reporting that more than 53,000 Chinese suspects linked to telecom and online fraud in northern Myanmar have been apprehended and brought back to China. Available at: <https://www.mps.gov.cn/n2255079/n4876594/n5104076/n5104077/c10056402/content.html>.

⁴UN Office of the High Commissioner for Human Rights, “Hundreds of thousands trafficked to work for online scammers in Southeast Asia,” 29 August 2023. Available at: <https://www.ohchr.org/en/press-releases/2023/08/hundreds-thousands-trafficked-work-online-scammers-se-asia-says-un-report>.

The unique geographic and political conditions in northern Myanmar have created a highly favorable environment for telecom fraud operations. Northern Myanmar lies right next to China, and a key feature of this area is the weak control exerted by Myanmar's central government. In practice, these regions bordering China are controlled by various ethnic minority armed groups and local forces, with many of the main controlling ethnic groups being predominantly Han Chinese (or ethnically Chinese). This governance vacuum has fostered illicit economies and transnational telecom fraud.

And one catalyst for the fraud boom in Northern Myanmar was a 2019 change in Myanmar's gambling policy. In May 2019, Myanmar's parliament enacted a new Gambling Law that legalized casino operations for foreign nationals. This opening of the casino industry – limited to foreign patrons – drew a surge of Chinese investment and personnel into border regions. Numerous casinos and related enterprises sprang up, quickly expanding into online gambling and scam operations under the guise of legal business. The promise of quick profits attracted tens of thousands of Chinese nationals to northern Myanmar (many entering through illicit channels), and even drove up the cost of making illegal fake border crossings pass from a few hundred yuan to tens of thousands. In effect, the 2019 casino legalization created an environment in which fraud groups could thrive with greater freedom.⁵

Another major factor was the collapse of central governance following the February 2021 military coup in Myanmar. The coup plunged the country into civil conflict thereby weakening central authority in outlying regions. In the ensuing power vacuum, local militias and ethnic armed factions in the north formed alliances with telecom fraud networks, providing these criminal operations with armed protection and territorial autonomy. Telecom fraud and online gambling quickly grew into major industries under militia patronage. This con-

⁵For discussions of how the 2019 Gambling Law, together with regional crackdowns on online casinos, enabled the relocation and rapid expansion of Chinese-facing casino and cyber-scam operations in northern Myanmar border enclaves such as Shwe Kokko/Yatai New City, see Global Initiative Against Transnational Organized Crime (2022), *Asian Roulette: Criminogenic Casinos and Illicit Trade in Environmental Commodities in South East Asia*, available at <https://globalinitiative.net/analysis/casino-crime-south-east-asia/>; and ISEAS–Yusof Ishak Institute (2020), *Shadow Capital at Myanmar's Margins: Shwe Kokko New City, Casinos and China's Role*, available at https://www.iseas.edu.sg/wp-content/uploads/2020/11/ISEAS_Perspective_2020_136.pdf.

vergence of political turmoil and lawlessness after 2021 greatly accelerated the expansion of fraud syndicates in northern Myanmar.

In summary, the combination of regulatory change in 2019 and post-coup governance collapse in 2021 fueled an unprecedented surge in telecom fraud across northern Myanmar. Accordingly, May 2019 is selected as the critical event timing for my empirical analysis, marking the onset of legalized foreigner-only casinos that catalyzed the telecom fraud industry's rise.

4 Analysis and Hypotheses

The core research question of my research is: What are the economic impacts of illegal immigration and cross-border criminal activities on local economics in border regions?

On the one hand, a significant influx of people into a region, even if associated with illicit activities or involving undocumented migration, can generate positive demand-side shocks in the short term. This population increase can stimulate local consumption, raising demand for essential goods and services such as basic housing, food, transportation, and retail items. Furthermore, if the fraud operations involve substantial financial flows, some portion might be injected into the local economy, further boosting short-term activity, albeit potentially concentrated in specific areas or sectors.

And individuals participating in or facilitating cross-border telecom fraud may actively seek less conspicuous locations to avoid detection by authorities. This could lead to concentrations of activity and residence not necessarily in established town centers, but perhaps in more peripheral or **remote villages and settlements within the border region**. The aggregate demand for necessities – including electricity consumption for living and potentially for operations, housing rentals, and local services – generated by this influx, dispersed across relatively less conspicuous locations near the border, could be plausibly shown as an increase in economic/human activities in this region. This perspective informs my first

hypothesis:

- **Hypothesis 1 (Positive Short-Term and Direct Effect):** The influx of population and associated activities linked to cross-border telecom fraud operations may *stimulate short-term local economic activity* in adjacent border regions, possibly concentrated in specific locations offering concealment.

On the other hand, the presence and intensification of large-scale organized criminal activities may exert negative pressure, although the specific mechanisms may differ by location. On the Myanmar side, where the telecom fraud operations are primarily concentrated, the direct presence of these major criminal enterprises can severely undermine the local rule of law, strain governance capacity, and potentially foster corruption, hindering normal and sustainable development. For the China side, while not hosting the bulk of the operations due to domestic enforcement, the primary negative economic channel likely operates through significant **reputational damage**. The widespread association of the border area with illicit activities and security concerns can tarnish its image. This negative reputation may deter legitimate economic engagement, particularly discouraging tourism and formal investment, as people might perceive higher risks related to safety and stability in the region. These perspectives lead to another hypothesis:

- **Hypothesis 2 (Negative Long-Term Reputational Indirect Effect):** The presence and intensification of illicit cross-border criminal operations may *undermine institutional quality* (especially where operations are concentrated) and damage the broader region's *reputation*, consequently *deterring legitimate economic activity (like tourism and investment) and hindering long-term growth*.

These two hypotheses capture the potential tension between short-term, demand-driven economic boosts and longer-term, potentially more damaging effects on the foundations of sustainable economic development.

5 Empirical Research 1: Grid-Level Nighttime Light Intensity

5.1 Data Description

In this section, I utilize a panel dataset of grid points (10km*10km) covering the border region from 2014 to 2024, with a total of 69,993 grid-year observations (6363 grids). And I began by identifying the 15 official border ports (border crossings) between China and Myanmar. Subsequently, the research area was then selected to encompass every grid point situated no more than 300 kilometers away from at least one of these identified crossings, as shown in Figure 1.

A significant challenge in this study is the data limitation. I do not have straightforward variable to measure the intensity or the extent of the economy and human activities, especially for the Myanmar side, where there not exist any official economic statistics. To overcome this data limitation, I employ nighttime light (NTL) intensity as my primary proxy variable for local economic and human activity intensity. NTL data, captured by satellites, has been increasingly recognized and validated in economic research as a powerful indicator of economic development, especially in contexts where conventional data is lacking (Henderson et al., 2012; Chen and Nordhaus, 2011). The intensity of nighttime illumination is strongly correlated with electricity consumption, infrastructure development, industrial output, and overall Gross Domestic Product (GDP) at various spatial scales (Donaldson and Storeygard, 2016). It effectively captures the geographic distribution and intensity of human activity, making it a suitable measure for my research question.

Specifically, I utilize data from the Visible Infrared Imaging Radiometer Suite (VIIRS) provided by Google Earth Engine (GEE), which offers improvements over older NTL datasets (like DMSP-OLS) in terms of spatial resolution, calibration, and saturation limits (Li and Zhou, 2017). My main outcome variable, therefore, is the annual average VIIRS NTL intensity for each grid point.

And for the treatment variable, I define the treatment intensity as the normalized negative distance to border crossing:

$$TreatmentStrength_i = -\frac{Distance_i - \overline{Distance}}{\sigma_{Distance}} \quad (1)$$

where $Distance_i$ is the distance from grid point i to the nearest official border crossing, $\overline{Distance}$ is the mean distance across all grid points in the sample, and $\sigma_{Distance}$ is the standard deviation of these distances.

The rationale for using distance to border crossings as a proxy for exposure to the impacts of Northern Myanmar's telecom fraud stems from several considerations. First, while the exact locations of the clandestine scam compounds are difficult to pinpoint, they are known to be geographically concentrated in regions of Northern Myanmar immediately adjacent to the Chinese border. Second, the large-scale nature of these fraud operations necessitates significant cross-border flows – including the movement of organizers and financiers entering Myanmar, the trafficking or luring of victims/workers into the compounds. These flows, both licit and illicit, are inherently concentrated around official crossings. Consequently, grid points closer to these nodes are likely to experience more intense effects.

Furthermore, I incorporate some control variables (latter I will multiple them with year dummy) including geographic features like slope and elevation, also the Normalized Difference Built-up Index (NDBI) which is a measure related to urbanization and infrastructure development. These geographic features are included as controls because they are strongly associated with baseline levels of human activity and development suitability; for example, areas with significantly higher elevations or steeper slopes often correspond to mountainous terrain, which typically limits large-scale settlement and economic infrastructure compared to lower-lying, flatter areas. And since NDBI primarily reflects longer-term patterns of built-up areas and infrastructure accumulation, I include it as a control variable representing baseline development levels, rather than treating it as a short-term outcome variable

potentially influenced by the event.

Table 1 presents the descriptive statistics for the key variables used in my analysis. The VIIRS nighttime light intensity exhibits a mean of 0.300 across the grid-year observations, but with substantial variation (standard deviation of 0.667). This large standard deviation highlights the significant heterogeneity in economic development and human activity levels across the border region. The NDBI, available from 2016 onwards in my dataset, shows a mean of -0.191 and a standard deviation of 0.075. The geographic controls also demonstrate considerable variability within the study region. Elevation averages 1382 meters (ranging widely from 70m to 4923m), and the average slope is relatively gentle at 1.79 degrees, also varying a lot (std. dev. 1.44, ranging from 0.004 to 9.547).

5.2 Empirical Methodology

To estimate the impact of proximity to the China-Myanmar border crossings on local economic activity, I employ a difference-in-differences (DiD) framework using my panel dataset covering grid cells i over years t . My primary specification utilizes a Two-Way Fixed Effects (TWFE) model:

$$Y_{it} = \beta \cdot TreatmentStrength_i \cdot Post_t + \mathbf{C}_{it} + \mu_t + \delta_i + \epsilon_{it} \quad (2)$$

where Y_{it} represents the VIIRS nighttime light intensity for grid cell i in year t . $TreatmentStrength_i$ is the time-invariant treatment intensity variable for grid i , defined as the standardized negative distance to the nearest official border crossing before. $Post_t$ is an indicator variable equal to 1 for the post-treatment years (e.g., $Post_t = \mathbf{1}\{Year_t > 2018\}$) and 0 otherwise. δ_i denotes grid point fixed effects, controlling for all time-invariant unobserved characteristics of each grid cell. μ_t represents year fixed effects, capturing common time shocks and aggregate trends affecting all cells. \mathbf{C}_{it} is a set of control variables, potentially including interactions with year dummies, detailed below. β is the coefficient of interest, representing the average

differential effect associated with treatment intensity in the post-treatment period. ϵ_{it} is the error term.

To assess the dynamics of the potential impact and examine the validity of the parallel trends assumption, I also estimate an event study model:

$$Y_{it} = \sum_{\tau \neq 2018} \beta_\tau \cdot TreatmentStrength_i \cdot \mathbf{1}\{Year_t = \tau\} + \mathbf{C}_{it} + \mu_t + \delta_i + \epsilon_{it} \quad (3)$$

In this specification, the single interaction term from Equation (2) is replaced by a series of interactions between the treatment intensity $TreatmentStrength_i$ and dummy variables $\mathbf{1}\{Year_t = \tau\}$ for each year τ in the sample period, relative to a baseline year (here, 2018 is omitted, serving as the reference year). The coefficients β_τ capture the year-specific differential changes relative to the baseline year 2018. Examining β_τ for years before the treatment period ($\tau < 2019$) provides a test for pre-existing trends, while coefficients for $\tau \geq 2019$ illustrate the post-treatment dynamics.

I implement these models with a progressively richer set of controls included in the term \mathbf{C}_{it} :

1. My base specification includes only grid point fixed effects (δ_i) and year fixed effects (μ_t), meaning $\mathbf{C}_{it} = 0$.
2. I then augment the model by adding interactions between year dummies and polynomial functions of time-invariant geographic characteristics (elevation and slope) for each grid cell i . This allows the effect of geography on Y_{it} to vary over time ($\mathbf{C}_{it} = \text{poly}(\text{Elevation}_i, \text{Slope}_i) \times Year_t$).
3. In a subsequent specification, I enhance the control for time-varying regional factors by replacing the year fixed effects (μ_t) with more granular province-by-year fixed effects (μ_{pt}).
4. Finally, my most comprehensive specification further incorporates interactions between

year dummies and polynomial functions of baseline (pre-treatment year 2018) control variables, specifically the 2018 VIIRS NTL and NDBI values for grid cell i , i.e.: $([\text{poly}(\text{Elevation}_i, \text{Slope}_i) + \text{poly}(VIIRS_{i,2018}, NDBI_{i,2018})] \times Year_t)$, used in conjunction with the appropriate set of fixed effects from step 3. This helps to control for differential trends related to initial development levels.

Standard errors in all regressions are clustered at the grid cell level (also adjust clustering level at province in 3 an 4). My preferred results typically come from the specifications including the comprehensive set of controls.

5.3 Baseline Results

Table 2 and Figure 3 presents the event study estimates for the effect of proximity to border crossings on nighttime light intensity. Several key patterns can be observed from this analysis.

The event study allows us to investigate this by examining the coefficients β_τ for the pre-treatment years (2014-2017). Ideally, these coefficients should be statistically indistinguishable from zero. As shown in Table 2, the estimates for the pre-2018 period are generally small and lack statistical significance, particularly in my preferred specification, Column (4). In Column (4), which incorporates grid point and province-by-year fixed effects, as well as interactions of year dummies with geographic features and baseline 2018 NTL/NDBI levels, none of the coefficients from 2014 to 2017 are statistically significant at conventional levels (t-statistics range from -1.591 to 0.934). This pattern provides strong support for the validity of the parallel trends assumption, suggesting no significant differential pre-existing trends related to my treatment variable in the years leading up to the reference period.

Comparing the results across the columns in Table 2 demonstrates the robustness of my main findings. While the inclusion of additional controls, particularly the province-by-year fixed effects (Column 3) and the interactions with baseline 2018 controls (Column 4), affects the magnitude and precision of the estimates, the overall pattern of post-treatment effects remains consistent. Specifically, a positive and statistically significant differential

effect emerges in the years following 2018/2019 across all specifications. This robustness increases confidence in the findings.

I focus my discussion on the results from Column (4), which represents the most comprehensive and preferred specification. The coefficients trace the dynamic evolution of the relationship between border crossing proximity and NTL intensity relative to 2018. I observe no very statistically significant differential effect in 2019 ($\beta_{2019} = 0.0036$, $t=1.668$). However, a positive and statistically significant effect emerges in 2020 ($\beta_{2020} = 0.0113$, $p < 0.01$). This suggests that, relative to 2018 and controlling for a wide array of factors, a one standard deviation increase in proximity (i.e., decrease in distance) to the nearest border crossing is associated with an approximately 0.011 unit increase in VIIRS NTL intensity starting in 2020. And later in next section I will show the percentage effect.

The estimated effect intensifies and persists in subsequent years. The coefficient increases to 0.0138 ($p < 0.01$) in 2021 and further to 0.0162 ($p < 0.01$) in 2022. The impact reaches its peak in the presented data in 2023, with a coefficient of 0.0226 ($p < 0.01$), indicating a substantial differential increase in NTL in areas closer to border crossings during this year. The effect remains strong and highly significant in 2024 ($\beta_{2024} = 0.0181$, $p < 0.01$). This temporal pattern suggests that the factors captured by proximity to border crossings began to exert a significant differential positive influence on local NTL intensity around 2020, with this influence growing markedly through 2023 and persisting into 2024.

In summary, the event study analysis, validated by the examination of pre-trends, reveals a statistically significant and robust positive association between proximity to China-Myanmar border crossings and nighttime light intensity, emerging from 2020 onwards. The magnitude of this differential effect grows substantially over the post-2019 period documented in my data. These findings suggest that the rise of telecom fraud activities in Northern Myanmar has had a significant positive effect on economic/human activities in areas closer to border crossings. The growing magnitude of the treatment effects over time indicates that the impacts of these activities have been persistent and cumulative, rather

than transitory.

5.4 Other Concerns

5.4.1 Concerns About COVID-19

It is important to acknowledge a major confounding event coinciding with my post-treatment period: the COVID-19 pandemic. Beginning in early 2020, the pandemic and subsequent public health responses, including widespread lockdowns, travel restrictions, and border closures, triggered significant negative shocks to global and regional economies. These effects were potentially more pronounced in border regions, given their reliance on cross-border trade, tourism, and movement of people – sectors severely impacted by pandemic restrictions.

This widespread negative economic shock could potentially bias my estimation of the treatment effect associated with border crossing proximity. Specifically, since the pandemic likely reduced overall economic activity and thus nighttime light intensity especially for border regions during the post-2019 period, it could exert a downward bias on my estimated coefficients (β in Equation (2) and β_τ in Equation (3)). In other words, the negative shock from COVID-19 might mask or reduce the magnitude of any positive differential effect captured by my treatment variable.

However, this potential downward bias is not a primary concern for the validity of my core findings. If, despite the dampening effect of the pandemic, we still identify statistically significant positive coefficients – as suggested by my event study results particularly from 2020 onwards – this indicates that my estimates are likely conservative. The persistence of a discernible positive effect, even amidst a major negative economic shock, would suggest that the findings are robust and potentially underestimate the true magnitude of the underlying effect absent the pandemic.

5.4.2 Spatial Spillover

An other potential concern in my setting is the presence of spillover effects. Activities or outcomes in one grid cell might influence outcomes in nearby cells, potentially violating the Stable Unit Treatment Value Assumption (SUTVA) crucial for causal inference. Such spatial correlation—whether positive, negative, or more complex—could arise if, for instance, economic activity is displaced from or attracted to areas based on their proximity to the border crossings, potentially biasing my main estimates from Equations (2) and (3). For example, if the spillover effect is positive, it could exert a downward bias since the difference between "treat" and "control" groups may be smaller.

To mitigate this concern about potential spillover bias, which can invalidate standard difference-in-differences estimates by affecting nearby control units, I implement an analysis using discretized levels of treatment intensity. Specifically, I divide my sample of grid cells into 10 equal-sized bins (deciles) based on their treatment intensity score ($TreatmentStrength_i$). Bin 1 contains the grid cells with the lowest treatment intensity (i.e., those typically furthest from crossings), while Bin 10 contains those with the highest intensity (closest proximity).

I designate Bin 1 as the control group for this analysis. Subsequently, I estimate nine separate DiD regressions. Each regression compares the outcomes (Y_{it}) in a specific "treated" bin (Bin k , where $k \in \{2, 3, \dots, 10\}$) to the outcomes in the control group (Bin 1), controlling for appropriate fixed effects and covariates. This procedure allows us to estimate the treatment effect specific to each intensity bin relative to the group presumed to be least directly affected. Figure 4 visually summarizes the setup or results of this approach.

This binning strategy serves two key purposes. First, by comparing groups with more distinct levels of treatment intensity, it may reduce potential bias stemming from spillovers that primarily affect neighboring cells or cells with similar intensity levels, which is analogous to the idea discussed by Butts (2023). Second, it explicitly examines potential non-linearities in the treatment effect, as the impact of proximity to border crossings might not change uniformly with distance. By estimating separate effects for each discrete intensity bin, we can

observe how the magnitude of the impact varies across the treatment intensity distribution.

While this method provides a valuable robustness check, I acknowledge that it may not entirely eliminate all forms of spillover bias. Spillovers could potentially occur across bins or even affect the control group (Bin 1) to some degree. Nevertheless, this disaggregated analysis likely offers a more nuanced understanding of the effects and helps to alleviate concerns in some extent.

5.5 Result Using the Bins as Treatment and Heterogeneity Analysis

The approach talked above compares grid cells in higher intensity bins (Bin 2 through Bin 10) to those in the lowest intensity bin (Bin 1 - furthest distance from crossings). Table 3 presents the estimated DiD coefficients for the overall sample, as well as separately for grid cells within China and Myanmar. Figures 5, 6, and 7 visualize these results.

Examining the Overall Sample (Table 3, top panel; Figure 5), a clear non-linear relationship emerges. The estimated effects for Bins 2 through 6 are statistically insignificant and centered around zero, suggesting that grid cells with low to moderate proximity experience no significant differential change in nighttime light (NTL) intensity compared to the furthest group (Bin 1). A positive effect begins to appear for Bin 7 (0.017, insignificant) and Bin 8 (0.023, $p < 0.1$), and it becomes statistically significant and economically meaningful for the two highest intensity bins: Bin 9 (0.051, $p < 0.01$) and Bin 10 (0.046, $p < 0.01$). These results indicate that the positive association between crossing proximity and NTL intensity is strongly concentrated in the areas closest to the border crossings, representing approximately a 14% increase relative to the pre-treatment (2018) mean NTL in those bins.

The analysis, when disaggregated by country, reveals some variations between the China and Myanmar samples (Table 3, middle and bottom panels; Figures 6 and 7). For instance, the China sample shows a significant negative coefficient for Bin 2, and the exact bin where positive effects become significant differs slightly from the Myanmar sample. And the treat-

ment effect for bin 8-10 is more significant for Myanmar side. However, despite these minor differences, the overall pattern of effects across the treatment intensity bins is remarkably similar on both sides of the border. This indicates a shared pattern where the impacts associated with proximity are strongly concentrated in the grid cells located closest to the official border crossings, regardless of which country they fall within.

This similarity in the spatial pattern of effects is plausible given the inherently cross-border nature of the telecom fraud activities in this region. Although the large-scale operational compounds are primarily situated on the Myanmar side of the border, the vast majority of the personnel involved—ranging from organizers to the extensive workforce—are reported to be Chinese nationals. These individuals typically cross the border, often illegally, to reach the compounds. Consequently, towns, villages, and transportation routes near the border crossings on both the Chinese and Myanmar sides inevitably serve as crucial transit points, logistical hubs, or recruitment grounds. This shared function as part of the essential cross-border infrastructure supporting the fraud industry likely explains why communities on both sides experience similarly concentrated impacts, particularly near the crossing points that facilitate this movement, resulting in the comparable non-linear patterns observed in my binned DiD analysis.

In conclusion, this binned DiD analysis, while revealing some minor variations, strongly supports the presence of a shared non-linear treatment effect related to border crossing proximity on both sides of the China-Myanmar border. The positive impacts on NTL intensity are primarily and consistently concentrated in the grid cells located closest to the crossings (highest intensity bins). This finding adds valuable nuance to my main results, reinforces the conclusion that effects are spatially concentrated near the border interface, and suggests that the impacts are linked more to the cross-border dynamics of personnel movement than strictly to the physical location of the scam compounds within Myanmar. It also increases some confidence that the observed effects are robust under potential spillover, though complex spillover dynamics cannot be entirely ruled out.

6 Emperical Research 2: City-Level Population Migration

6.1 Data Description

Building upon the previous analysis which examined localized economic activity proxies using grid-level data, this second part of my research shifts focus to investigate potential impacts on a different dimension: human mobility at a broader spatial scale. I utilize monthly city-level migration data for relevant cities in China covering the period from 2018 to 2022. The analysis aims to assess whether the intensification of telecommunications fraud activities in northern Myanmar influenced population mobility patterns, particularly in adjacent Chinese border cities.

The migration data is provided by Gaode Maps, a major provider of navigation and location-based services in China. I obtained monthly city-level indices capturing population mobility: specifically, **a migration inflow index, a migration outflow index, and a net migration inflow index** for each city. These indices are generated by tracking the movements of users; when an individual has the Gaode Map application installed and location services activated, the platform can log their cross-city travel. Therefore, the inflow and outflow indices serve as proxies for the volume of population movement, roughly corresponding to the relative scale of person-trips entering and leaving a city each month. While presented as indices, the magnitude can often be roughly considered as 'tens of thousands of person-trips'. The net migration index is directly derived as the difference between the inflow and outflow indices for each city-month observation.

My empirical strategy relies on a Synthetic Control approach, necessitating careful definition of treatment and control groups based on geographic closeness to the northern Myanmar border region. The **Treatment Group** consists of six cities in Yunnan province that share a border with Myanmar. These units are: **Baoshan, Puer, Lincang, Dehong Dai and Jingpo Autonomous Prefecture, Nujiang Lisu Autonomous Prefecture, and**

Xishuangbanna Dai Autonomous Prefecture (see Figure 8).

Recognizing the spillover that effects might not be strictly confined to the immediate border cities, I define a **Potential Spillover Group**. This group comprises the remaining cities within Yunnan province that are not included in the treatment group. The **Control Group** is then designed as other cities outside Yunnan. And later the SCM will choose the controls for each treated city only inside the Control Group.

Table 4 provides descriptive statistics for the key quarterly migration indices, presented separately for the Treatment and Spillover groups and divided into the pre-treatment (2018Q2-2019Q1) and post-treatment (2019Q2-2022Q4) periods.

6.2 Empirical Methodology

Two primary concerns guide the methodological choices. First, the small number of treated units in my analysis poses a challenge for traditional difference-in-differences (DiD) estimators. my **treatment group consists of only six** cities in Yunnan. Conventional DiD methods often rely on comparing averages across larger treatment and control groups, and their statistical power and the reliability of identifying assumptions can be limited when dealing with such a small number of treated units ($N_T = 6$). To address this, I require a method well-suited for comparative case studies with few treated units, capable of constructing a credible counterfactual specifically tailored to each individual treated city. This motivates my use of the Synthetic Control Method (SCM), which is designed precisely for such settings. SCM creates a data-driven counterfactual for each treated unit by finding an optimal weighted combination of units from a larger donor pool.

Second, the **confounding influence of the COVID-19 pandemic** significantly overlaps with my post-treatment period (2019Q2 onwards) as discussed before. The pandemic induced major negative shocks, particularly to sectors like tourism and cross-border trade that are often vital for border economies. Unlike contexts where a downward bias might be considered conservative, in migration analysis, this could potentially be a problem since

the fraud activities may also have negative effect which can be seen later. The presence of such a strong, concurrent shock necessitates methods capable of isolating the specific effect of interest from aggregate time trends.

To handle the challenges mentioned above, my "manual" SCM approach emphasizes achieving a close pre-treatment match on variables crucial for understanding migration dynamics and city structure. Specifically, I configure the SCM optimization to minimize the discrepancy between the treated city i and its synthetic counterpart across the following pre-treatment variables:

1. Pre-treatment monthly trends (all periods $t \leq T_0$) of the Migration Inflow Index ($Y^{(1)}$).
2. Pre-treatment monthly trends of the Migration Outflow Index ($Y^{(2)}$).
3. Pre-treatment monthly trends of the Net Migration Inflow Index ($Y^{(3)}$).
4. Pre-treatment monthly trends of the Per-Capita Migration Inflow Index

$$Y^{(4)} = \frac{Y^{(1)}}{\text{Population}_{2018}},$$

where population refers to registered population.

5. The pre-treatment level (2018) of the proportion of Tertiary Industry in GDP ($X^{(5)}$).

Matching on the core migration trends (variables 1-3) ensures the baseline dynamics are captured. Furthermore, by explicitly matching on per-capita inflow trends (variable 4) and the pre-treatment share of the tertiary industry (variable 5), I aim to construct a synthetic control that shares a more similar underlying socio-economic structure and relative mobility intensity with the treated city prior to 2019Q2. Aligning these specific characteristics is crucial for enhancing the credibility of the counterfactual, particularly given the concurrent COVID-19 pandemic. Ensuring similarity in baseline per-capita mobility patterns and economic structure makes it more likely that the synthetic control would react similarly to the

treated city in response to large-scale, potentially sector-specific shocks like the pandemic, thus helping to isolate the treatment effect of interest from these confounding influences.

Formally, for each treated city i , I find the vector of weights $W_i = (w_{i,I+1}, \dots, w_{i,I+J})$ for the J cities in the donor pool (indexed $j = I + 1$ to $I + J$) that solves:

$$\min_{W_i} \sum_{m=1}^4 v_m \sum_{t=1}^{T_0} \left(Y_{i,t}^{(m)} - \sum_{j=I+1}^{I+J} w_{i,j} Y_{j,t}^{(m)} \right)^2 + v_5 \left(X_{i,5} - \sum_{j=I+1}^{I+J} w_{i,j} X_{j,5} \right)^2 + \lambda \sum_{j=I+1}^{I+J} w_{i,j}^2 \quad (4)$$

subject to the constraints that $w_{i,j} \geq 0$ for all j and $\sum_{j=I+1}^{I+J} w_{i,j} = 1$.

Here, $Y_{i,t}^{(m)}$ and $X_{i,5}$ are the values of the matching variables for the treated unit i , while $Y_{j,t}^{(m)}$ and $X_{j,5}$ are the values for control unit j . The hyperparameters $v_m \geq 0$ ($m = 1..5$) represent the relative importance placed on matching each specific predictor variable, allowing customization of the fit. The term governed by hyperparameter $\lambda \geq 0$ is an optional L2 regularization penalty on the weights, used to encourage using more cities rather than concentrating the weight heavily on only a few controls, which helps improve the generalization of the synthetic control and prevent overfitting. The optimal weights $w_{i,j}^*$ are then used to construct the synthetic control's outcome trajectory: $\hat{Y}_{it}^{SC} = \sum_{j=I+1}^{I+J} w_{i,j}^* Y_{jt}$. The SCM estimate of the treatment effect for treated city i at time t is $\hat{\tau}_{it}^{SC} = Y_{it} - \hat{Y}_{it}^{SC}$ for $t > T_0$. The overall average treatment effect for the treated group in a given post-treatment period t is then calculated by averaging these individual effect estimates across the six treated cities ($N_T = 6$).

While my customized SCM aims for an excellent pre-treatment fit by focusing on key variables, the match might still be imperfect. To address this, I also employ the Augmented Synthetic Control Method (ASCM) proposed by Ben-Michael et al. (2021).

ASCM builds upon the standard SCM by incorporating an outcome model estimated on the control units to predict and adjust for bias. The key steps are conceptually as follows:

- (1) Estimate the standard SCM weights W^* and the synthetic control \hat{Y}_{it}^{SC} as described above.

- (2) Calculate the pre-treatment residuals: $\varepsilon_t = Y_{it} - \hat{Y}_{it}^{SC}$ for $t \leq T_0$. These represent the deviations between the treated unit and its synthetic counterpart before the treatment.
- (3) Model these pre-treatment residuals ε_t using the outcomes of the units in the donor pool, Y_{jt} for $j = I+1 \dots I+J$ and $t \leq T_0$. This step often involves regularized regression (Here I use Ridge) to estimate a relationship \hat{f} such that $\varepsilon_t \approx \hat{f}(Y_{I+1,t}, \dots, Y_{I+J,t})$.
- (4) Use the estimated relationship \hat{f} and the post-treatment outcomes of the donor pool units to predict the likely trajectory of the residuals (i.e., the bias) in the post-treatment period: $\hat{\delta}_t = \hat{f}(Y_{I+1,t}, \dots, Y_{I+J,t})$ for $t > T_0$.
- (5) Adjust the standard SCM prediction by adding the estimated bias: $\hat{Y}_{it}^{ASC} = \hat{Y}_{it}^{SC} + \hat{\delta}_t$ for $t > T_0$. This \hat{Y}_{it}^{ASC} is the ASCM counterfactual.
- (6) Estimate the ASCM treatment effect as the difference between the observed outcome and the adjusted counterfactual: $\hat{\tau}_{it}^{ASC} = Y_{it} - \hat{Y}_{it}^{ASC}$ for $t > T_0$.

By leveraging the information contained in the outcomes of the control units to correct for imbalances and potential time-varying confounding, ASCM aims to provide estimates that are less sensitive to imperfect pre-treatment fit and potentially more robust than standard SCM.

6.3 Results for Treatment

This section presents the estimated effects of the telecommunications fraud activities in northern Myanmar on population mobility in the six treated Chinese border cities, using the Augmented Synthetic Control Method (ASCM). The results for the primary outcome variables – the monthly migration inflow, outflow, and net inflow indices – are visualized in Figure 9, Figure 10, and Figure 11. For each index, the left panel displays the trend of the actual treated cities (averaged) compared to their synthetic counterfactual (\hat{Y}_{it}^{ASC}), while the

right panel shows the estimated treatment effect over time. The vertical dashed line marks the beginning of the post-treatment period in May 2019.

The findings consistently suggest a notable decline in recorded population mobility for the treated border cities following the onset of the treatment period. For example, examining the **Migration Inflow Index** (Figure 9), the estimated treatment effect ($\hat{\tau}_{it}^{\text{ASC}}$, shown in the right panel) turns negative shortly after May 2019 and remains persistently below zero for most of the subsequent period. Specifically, the estimated negative gap typically fluctuates in the range of approximately -10 to -20 index points during the post-treatment years. Considering that the approximate pre-treatment Migration Inflow Index for these treated cities was around 16.25 (Table 4), and about 30 for the synthetic counterfactual after event, this estimated reduction represents a substantial negative impact. This indicates that migration into the treated cities was significantly lower than the counterfactual scenario predicted by the synthetic control group composed of unaffected cities. And the result about **Migration Outflow Index** is similar, while the **Migration Net Inflow Index** does not show a obvious pattern.

One primary consideration of the results is that the migration indices derived from Gaode Maps may not capture the movement of individuals directly involved in the illicit cross-border telecom fraud activities. Such individuals often take precautions to avoid digital tracking, for instance, by disabling location services on their smartphones. Therefore, the observed decline in recorded mobility likely reflects changes among the general population not directly involved in the fraud operations themselves. Therefore the results may indicate a decline in *legitimate* mobility. The increased salience and negative reputation associated with the region due to the widely publicized fraud activities, coupled perhaps with enhanced security concerns, could have deterred legitimate travel purposes, such as business trips, tourism, or regular migration intentions, leading to reduced inflows and outflows captured by the platform. Regardless of the precise mechanism, the findings point towards a negative shock to recorded population mobility in the affected border cities subsequent to the intensification

of nearby telecom fraud.

6.4 Robustness and Placebo Check

To further validate my main findings for the treated border cities and explore potential spillovers, I conduct two additional analyses: an assessment of effects on other cities within Yunnan province (Figure 12, Figure 13, and Figure 14), and a placebo test using 10 randomly selected control cities (Figure 15, Figure 16, and Figure 17).

First, I examine potential spillover on migration patterns in cities within Yunnan province that were not directly adjacent to the northern Myanmar border region and thus not included in my primary treatment group. These "spillover cities" might experience indirect impacts due to intra-provincial connections. I applied the ASCM analysis treating the average of this group as the unit of interest. Across the three indices for these spillover cities, the estimated treatment effects (gaps) appear relatively small compared to the baseline mobility levels. For **Migration Inflow** and **Migration Outflow**, the gap exhibit a slight negative tendency after event, potentially averaging around -10 to -15 index points. Conversely, the **Net Migration Index** gap fluctuates and might average slightly positive, perhaps around +5 index points. However, considering that the overall levels for inflow and outflow indices in these spillover cities were substantially higher, averaging around lager than 100, these estimated spillover effects represent only a minor deviation relative to the overall scale of mobility.

Second, I perform a placebo test to assess the reliability of my ASCM methodology and rule out the possibility that my main results are driven by chance. For this test, I randomly selected 10 cities from my designated control group (cities outside Yunnan) and applied the identical ASCM procedure, treating them as if they had received the treatment starting in 2019Q2. The estimated "treatment effects" for inflow, outflow, and net inflow indices remain centered around zero, exhibiting no discernible pattern following the pseudo-treatment date. The absence of a spurious effect in this placebo group may strengthens the confidence that

the negative effects on inflow and outflow detected for the actual treated border cities are indeed associated with the event.

7 Discussion and Conclusion

This paper investigated the multifaceted economic impacts of intensified cross-border telecommunications fraud activities in northern Myanmar on the adjacent China-Myanmar border region, utilizing two distinct empirical approaches. The first study, employing grid-level nighttime light (NTL) data from 2014-2024, found robust evidence of a positive association between proximity to border crossings and NTL intensity, particularly emerging and growing from 2019 onwards. This effect was non-linear and highly concentrated in areas closest to the crossings on both sides of the border. These findings lend support to the **Hypothesis 1**, suggesting that the influx of population and associated activities, potentially concentrated in specific settlements near the border for concealment or logistical reasons, might generate extra localized demand and activity to stimulate observable increases in the economic/human activity proxy (NTL).

However, my second study, examining city-level migration patterns in Chinese border cities from 2018-2022 using Augmented Synthetic Control Methods (ASCM), revealed a contrasting picture regarding population mobility. I found significant evidence of a decline in recorded migration inflow and outflow for the six treated border cities relative to their synthetic counterfactuals after the intensification event in May-2019. This reduction in recorded mobility aligns with the **Hypothesis 2**, suggesting that the broader region or the cities themselves may suffer from significant negative consequences, likely driven by **reputational damage**. As discussed, the migration data likely fails to capture illicit cross-border movements but reflects a decline in legitimate mobility, plausibly as tourism and business activities were deterred by safety concerns and the negative image associated with the region's widely publicized issues with fraud and crime.

Nonetheless, this research has several important limitations. First, the analysis relies on proxy measures for both illicit activity and local economic conditions. The absence of reliable micro-level data on telecom-fraud operations and formal economic statistics on the Myanmar side means that NTL and mobile phone-based migration indices inevitably capture a mix of relevant and irrelevant signals. Second, identification may still be affected by concurrent shocks and spillovers. In particular, the COVID-19 pandemic overlaps with much of the post-2019 period and, despite my attempts to mitigate its influence, could interact with the treatment in ways that are difficult to fully disentangle. Moreover, spatial spillovers across nearby locations or cities may violate standard “no interference” assumptions and bias the estimated effects. Third, both NTL and migration indices have intrinsic limitations as proxies: NTL responds more readily to certain types of activity than others, and Gaode-based migration measures do not capture illicit or offline movements that intentionally avoid digital tracking. Future research could draw on richer microdata, alternative remotely sensed indicators, or sector-specific outcomes (e.g., tourism, trade, real estate) to better isolate mechanisms and more precisely quantify the heterogeneous impacts of cross-border telecom fraud.

References

- Aldeco Leo, L., Jurado, A., and Ramírez-Álvarez, A. A. (2024). Internal migration and drug violence in mexico. *Journal of Development Economics*, 171:103334.
- Basu, S. and Pearlman, S. (2017). Violence and migration: Evidence from mexico’s drug war. *IZA Journal of Development and Migration*, 7(18). Open Access.
- Ben-Michael, E., Feller, A., and Rothstein, J. (2021). The augmented synthetic control method. *Journal of the American Statistical Association*, 116(536):1789–1803.

- Blattman, C., Duncan, G., Lessing, B., and Tobón, S. (2024). Gang rule: Understanding and countering criminal governance. *The Review of Economic Studies*, page rdae079.
- Butts, K. (2023). Difference-in-differences estimation with spatial spillovers.
- Chen, X. and Nordhaus, W. D. (2011). Using luminosity data as a proxy for economic statistics. *Proceedings of the National Academy of Sciences*, 108(21):8589–8594.
- Dell, M. (2015). Trafficking networks and the mexican drug war. *American Economic Review*, 105(6):1738–1779.
- Donaldson, D. and Storeygard, A. (2016). The view from above: Applications of satellite data in economics. *Journal of Economic Perspectives*, 30(4):171–98.
- Henderson, J. V., Storeygard, A., and Weil, D. N. (2012). Measuring economic growth from outer space. *American Economic Review*, 102(2):994–1028.
- Li, X. and Zhou, Y. (2017). A comparative analysis of dmsp/ols and viirs ntl data in coordinating development research for china's cities. *Remote Sensing*, 9(10):1075.
- MacBeath, A. (2025). Cashing in on conflict: Illicit economies and the myanmar civil war. *Global Initiative Against Transnational Organized Crime*.
- Melnikov, N., Schmidt-Padilla, C., and Sviatschi, M. M. (2025). Gangs, labor mobility, and development. Nova SBE Working Paper Series No. 672.
- Peng, X. (2024). Playing with fire: How engagement with illicit economies shapes the survival and resilience of ethnic armed organisations in the china-myanmar borderlands. *China Perspectives*, 138:9–20.
- Pinotti, P. (2015). The economic costs of organised crime: Evidence from southern italy. *The Economic Journal*, 125(586):F203–F232.

Uribe, A., Lessing, B., Schouela, N., and Stecher, E. (2022). Criminal governance in latin america: An assessment of its prevalence and correlates. *SSRN Electronic Journal*.

Figures

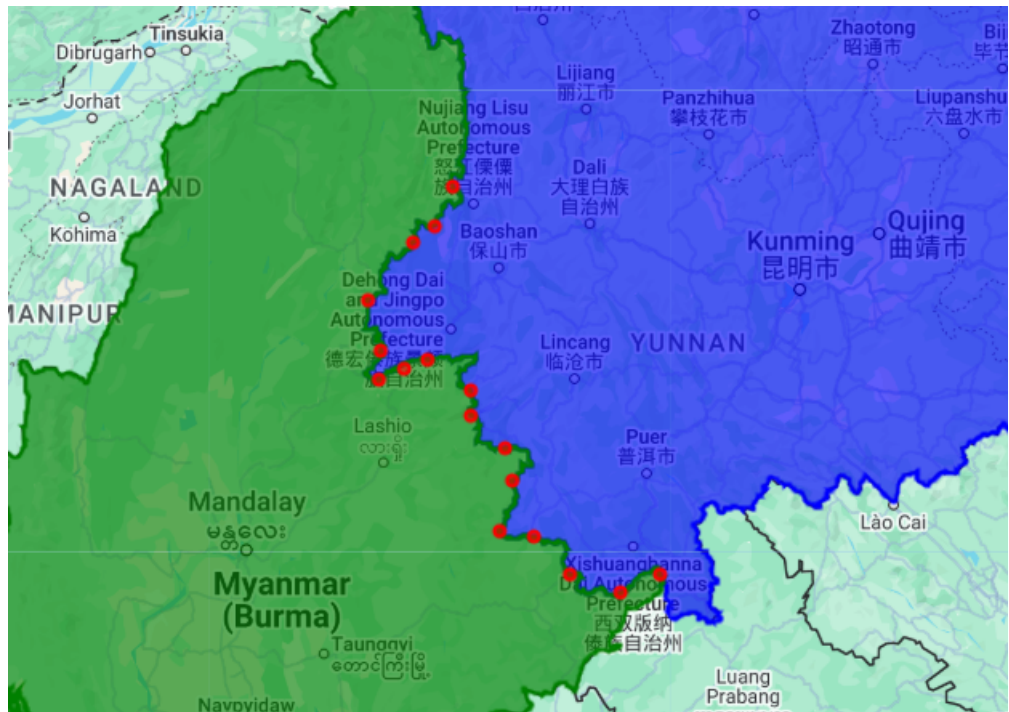


Figure 1: Study Region

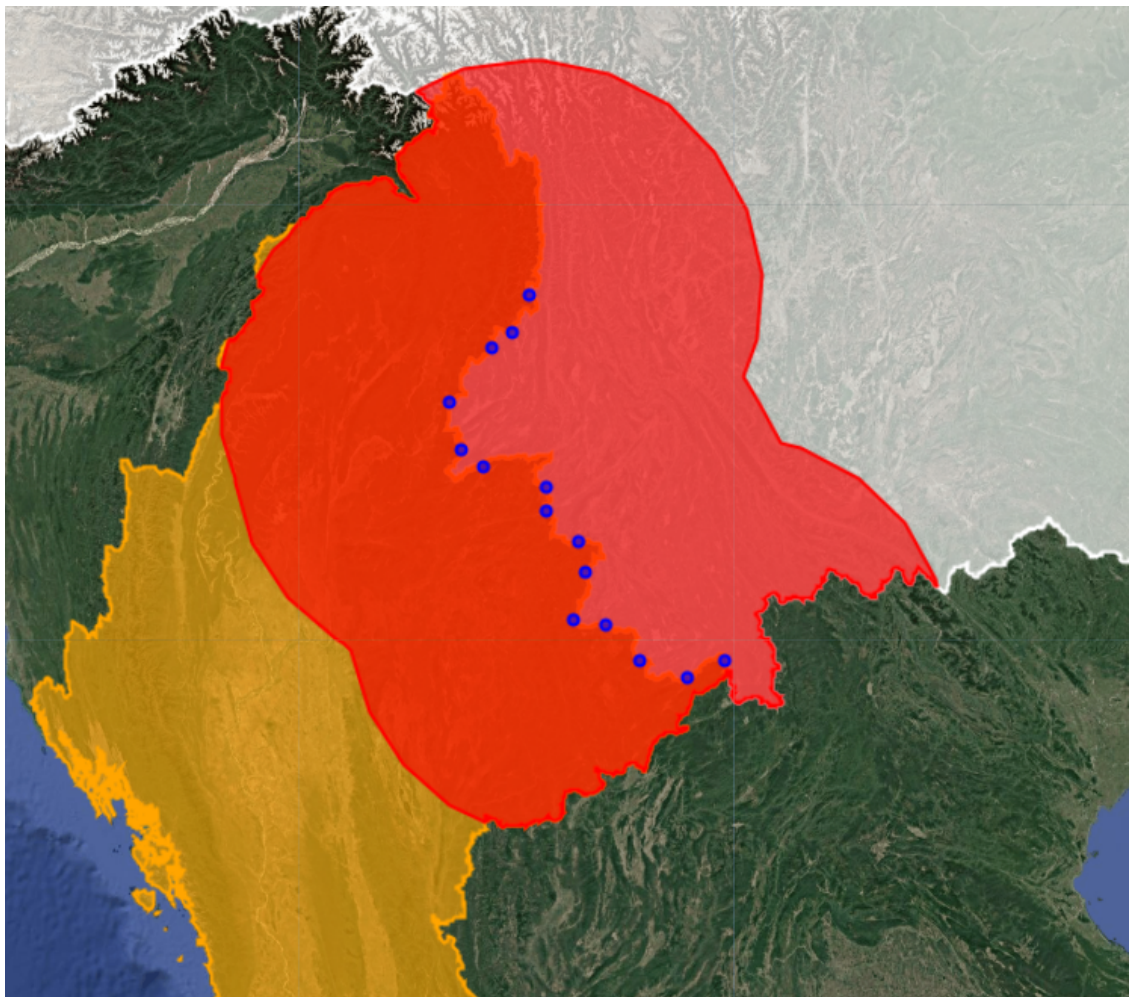


Figure 2: Study Region with Treatment Intensity

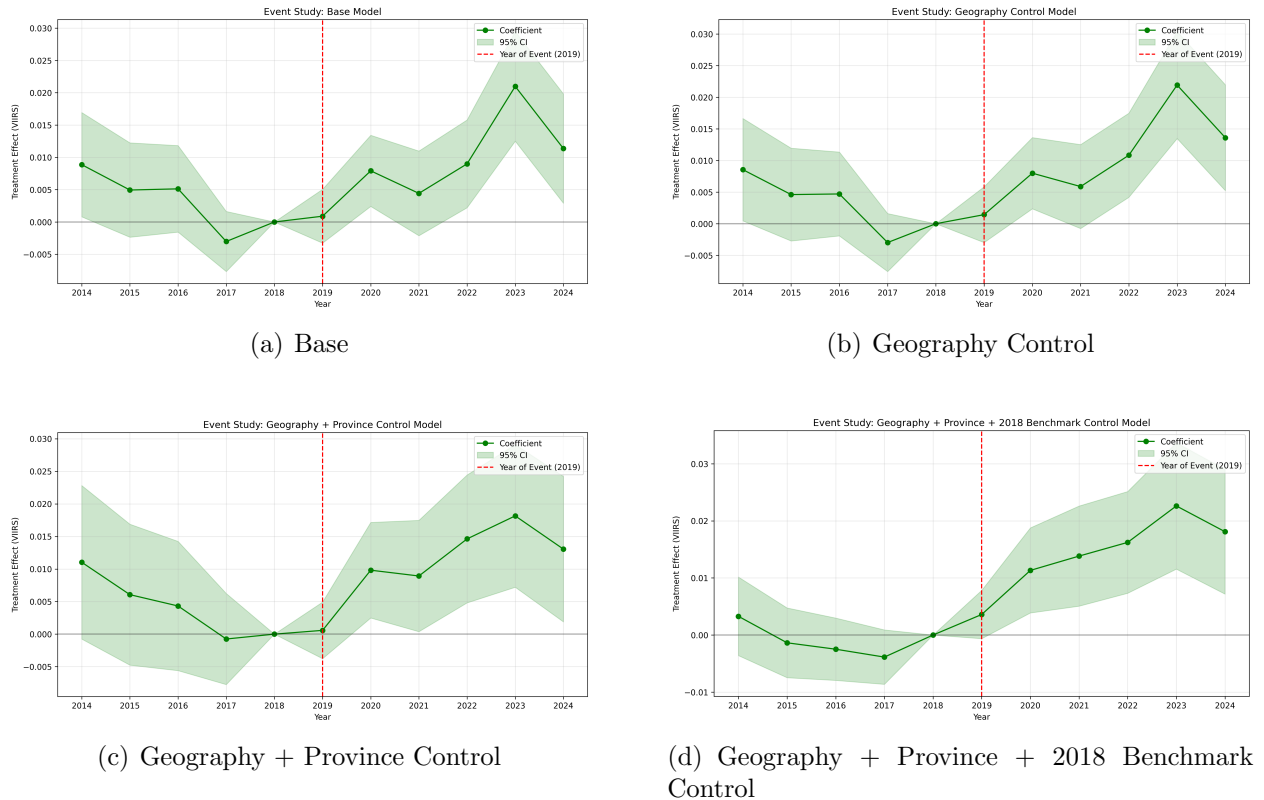


Figure 3: Event Study Analysis: The Effect of Border-Crossing Distance on Nighttime Light Intensity

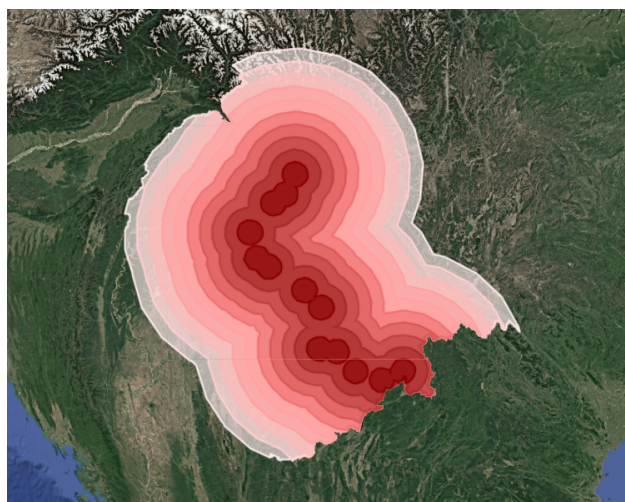


Figure 4: Bin of The Treatment Intensity

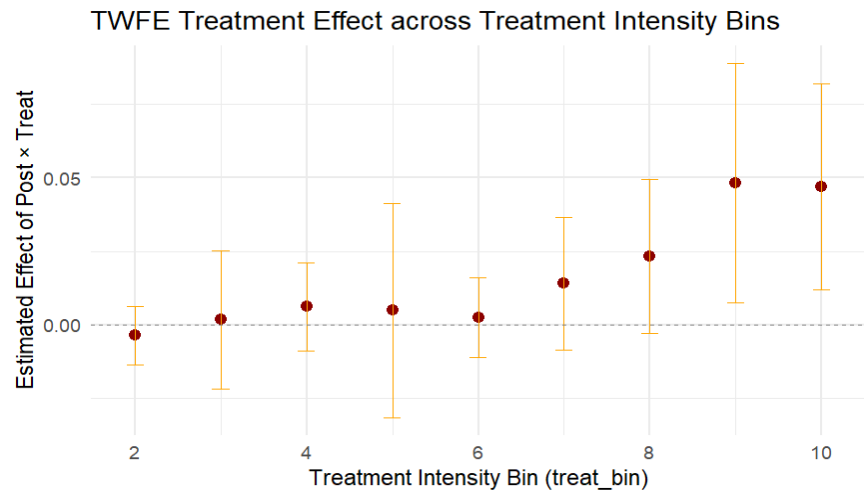


Figure 5: Treatment Effect across Bins: Total

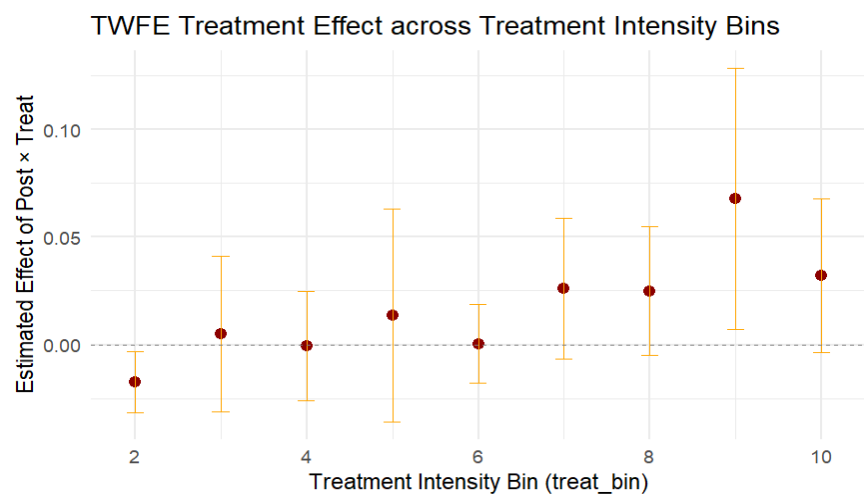


Figure 6: Treatment Effect across Bins: China

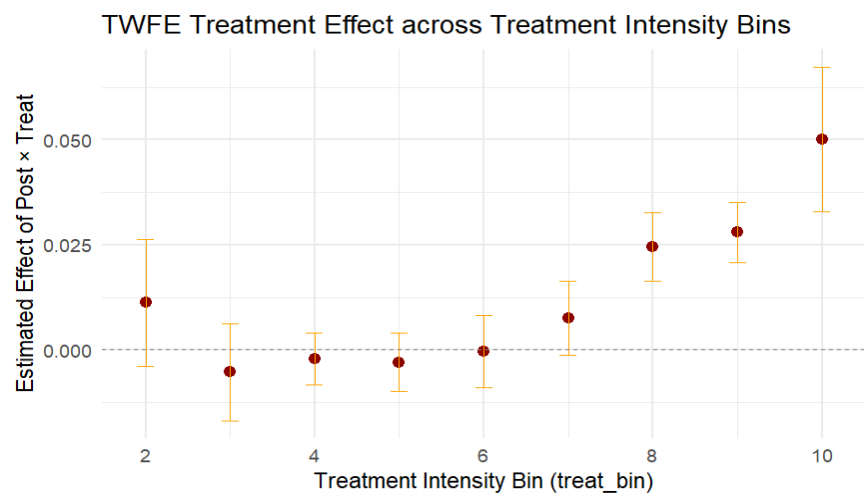


Figure 7: Treatment Effect across Bins: Myanmar



Figure 8: Treatment Cities: Yunnan Province

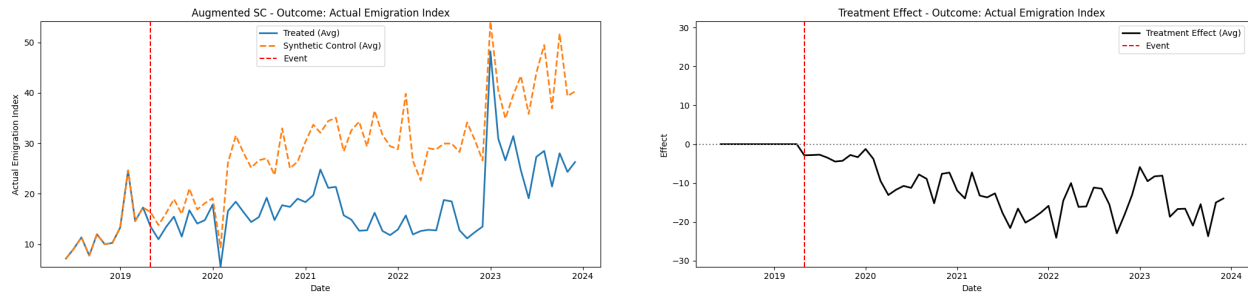


Figure 9: ASCM Results for Treatment Cities: Migration Inflow Index

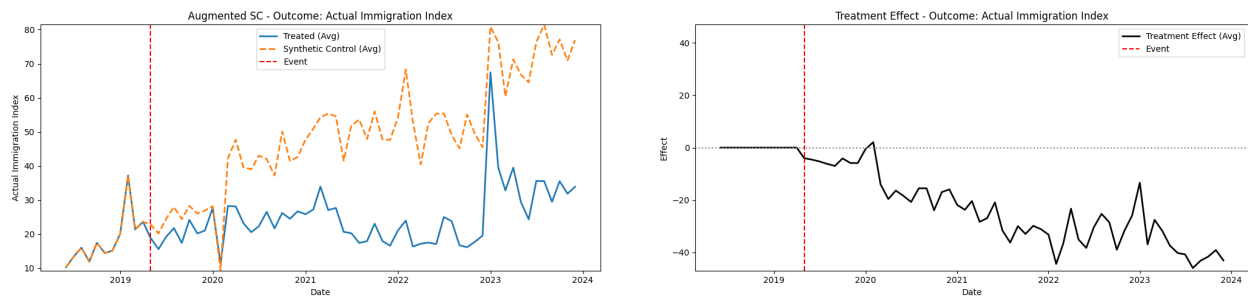


Figure 10: ASCM Results for Treatment Cities: Migration Outflow Index

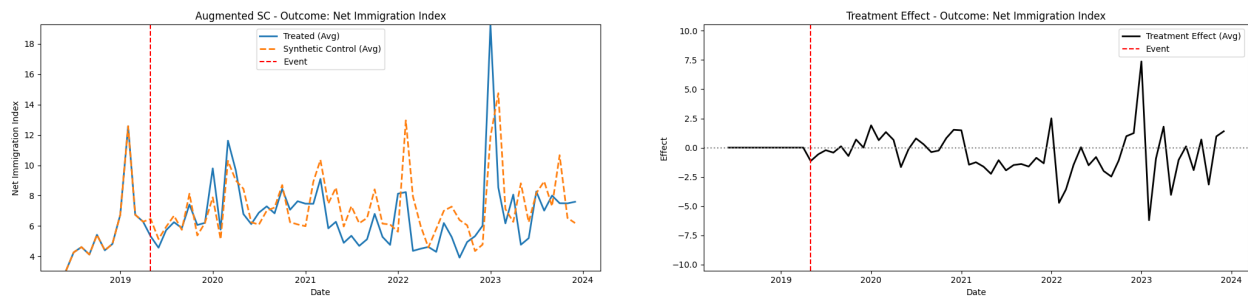


Figure 11: ASCM Results for Treatment Cities: Net Migration Index

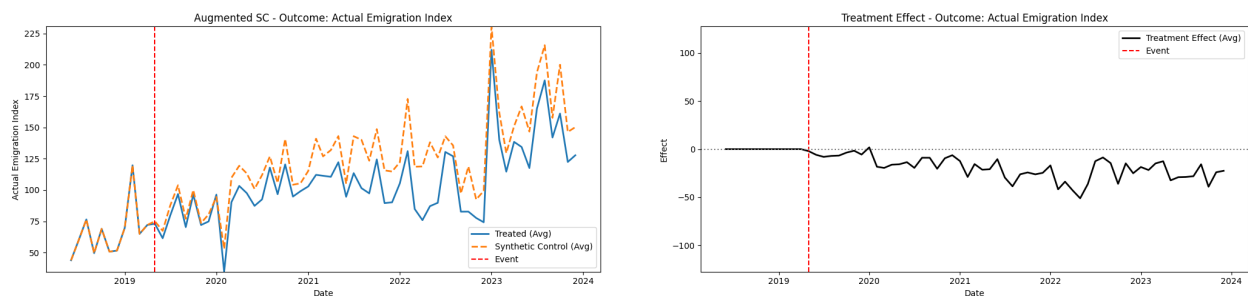


Figure 12: ASCM Results for Spillover Cities: Migration Inflow Index

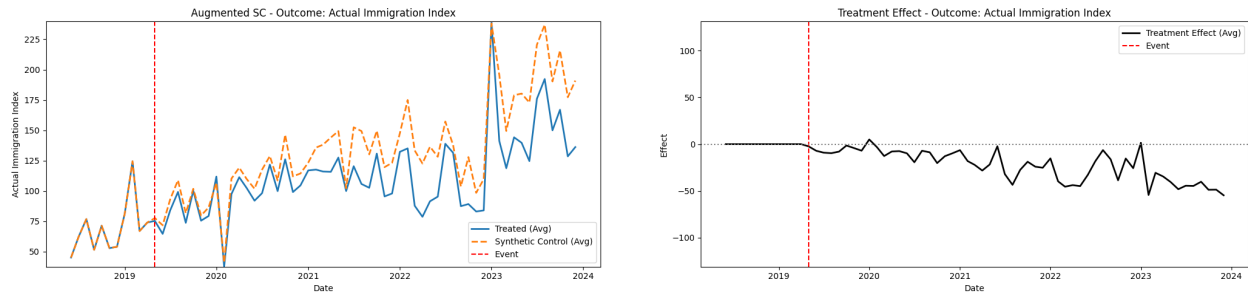


Figure 13: ASCM Results for Spillover Cities: Migration Outflow Index

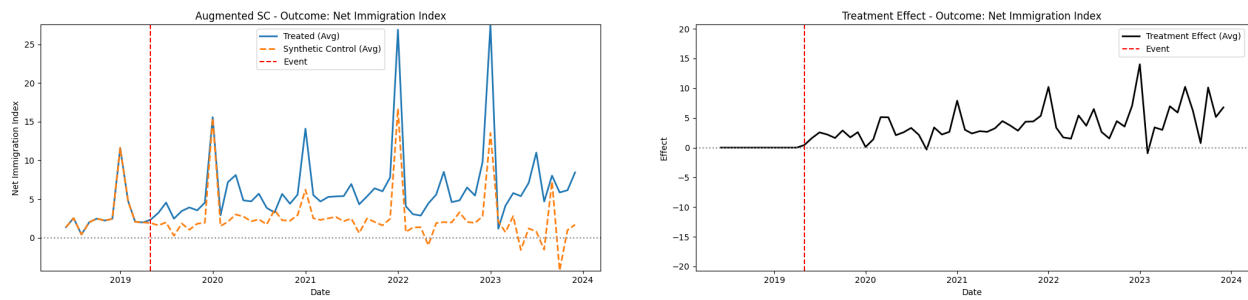


Figure 14: ASCM Results for Spillover Cities: Net Migration Index

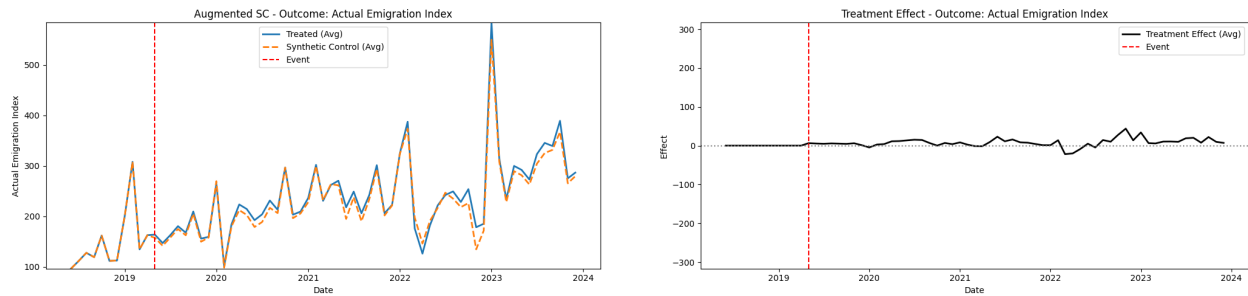


Figure 15: ASCM Results for Placebo Cities: Migration Inflow Index

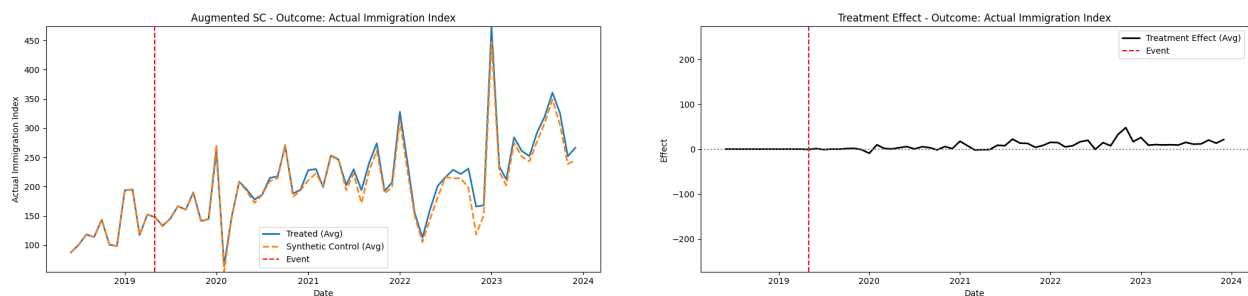


Figure 16: ASCM Results for Placebo Cities: Migration Outflow Index

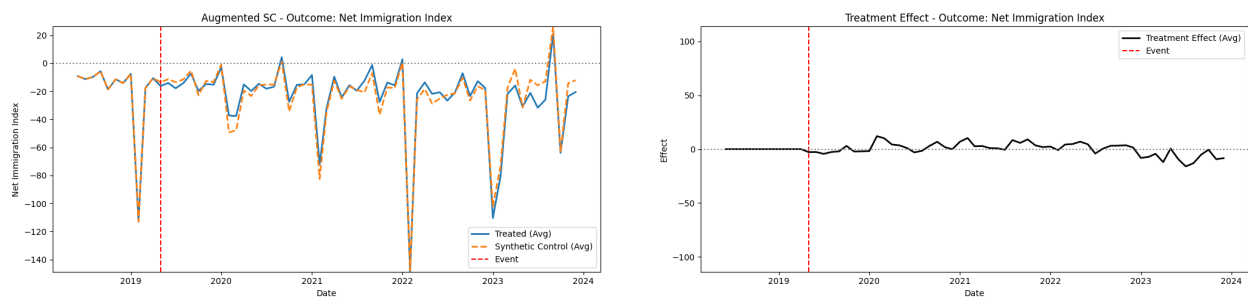


Figure 17: ASCM Results for Placebo Cities: Net Migration Index

Tables

Table 1: Descriptive Statistics for Key Variables

Variable	Obs	Mean	Std. Dev.	Min	Median	Max
VIIRS	69,993	0.300	0.667	-0.020	0.248	24.434
Distance to Border (km)	69,993	129.32	85.25	0.007	122.11	302.68
Distance to Crossing (km)	69,993	158.61	85.92	1.607	161.41	305.68
Elevation (m)	69,993	1,382	936	70	1,213	4,923
Slope (degrees)	69,993	1.79	1.44	0.004	1.45	9.55
NDBI	61,271	-0.191	0.075	-0.710	-0.191	0.258

Notes: This table presents descriptive statistics for key variables used in the grid-level analysis. Distances are converted to kilometers for readability.

Table 2: The Effect of Border Crossing Distance on Nighttime Light Intensity: An Event Study

	(1) Base	(2) Geo	(3) Geo+Prov	(4) Geo+Prov+2018
Crossing Proximity × Year 2014	0.0089** (2.155)	0.0086** (2.070)	0.0110* (1.835)	0.0033 (0.934)
Crossing Proximity × Year 2015	0.0049 (1.327)	0.0046 (1.231)	0.0061 (1.098)	-0.0014 (-0.438)
Crossing Proximity × Year 2016	0.0051 (1.501)	0.0047 (1.391)	0.0043 (0.854)	-0.0025 (-0.893)
Crossing Proximity × Year 2017	-0.0030 (-1.273)	-0.0030 (-1.273)	-0.0007 (-0.210)	-0.0039 (-1.591)
Crossing Proximity × Year 2019	0.0009 (0.421)	0.0014 (0.636)	0.0006 (0.261)	0.0036* (1.668)
Crossing Proximity × Year 2020	0.0079*** (2.817)	0.0080*** (2.780)	0.0098*** (2.624)	0.0113*** (2.978)
Crossing Proximity × Year 2021	0.0044 (1.325)	0.0059* (1.735)	0.0089** (2.048)	0.0138*** (3.091)
Crossing Proximity × Year 2022	0.0090*** (2.595)	0.0108*** (3.190)	0.0146*** (2.919)	0.0162*** (3.571)
Crossing Proximity × Year 2023	0.0210*** (4.847)	0.0219*** (5.080)	0.0182*** (3.249)	0.0226*** (4.005)
Crossing Proximity × Year 2024	0.0114*** (2.631)	0.0136*** (3.183)	0.0131** (2.291)	0.0181*** (3.247)
Observations	69,993	69,993	69,993	69,993
R ²	0.355	0.357	0.368	0.551
Entity FE	Yes	Yes	Yes	Yes
Time FE	Yes	Yes	Yes	Yes
Geography × Year	No	Yes	Yes	Yes
Province × Year	No	No	Yes	Yes
2018 Controls × Year	No	No	No	Yes

Notes: This table reports event study estimates. The treatment intensity is the negative standardized distance to the nearest border crossing. T-statistics in parentheses. Standard errors clustered at grid level. * p<0.1, ** p<0.05, *** p<0.01

Table 3: DID Effects across Treatment Intensity Bins

Panel A: Overall Sample					
Bin	2-3	4-5	6-7	8	9-10
Estimate	0.000	0.001	0.011	0.023*	0.049***
Std. Error	(0.008)	(0.013)	(0.009)	(0.012)	(0.018)
Pre-treatment Mean	0.304	0.324	0.272	0.251	0.304
Relative Effect	0.0%	0.3%	3.5%	8.5%	13.8%
Panel B: China Sample					
Estimate	-0.006	0.007	0.013	0.025	0.050**
Std. Error	(0.013)	(0.019)	(0.013)	(0.015)	(0.025)
Pre-treatment Mean	0.291	0.438	0.318	0.274	0.367
Relative Effect	-2.1%	1.4%	3.8%	8.3%	11.7%
Panel C: Myanmar Sample					
Estimate	0.003	-0.002	0.004	0.025***	0.039***
Std. Error	(0.007)	(0.004)	(0.004)	(0.004)	(0.007)
Pre-treatment Mean	0.317	0.240	0.238	0.234	0.245
Relative Effect	0.9%	-1.0%	1.5%	9.5%	13.5%

Notes: Bins grouped for presentation. Treatment effects relative to Bin 1 (furthest from border). * p<0.1,
** p<0.05, *** p<0.01

Table 4: Descriptive Statistics of Monthly Migration Indices

Variable	Mean	SD	Min	P25	Median	P75	Max
Treatment Cities							
<i>Pre-treatment (2018Q2-2019Q1)</i>							
Inflow Index	17.70	11.05	4.04	11.50	16.25	21.66	72.53
Outflow Index	12.02	9.13	1.56	6.24	9.51	16.05	50.88
Net Migration	5.68	6.80	-9.78	2.60	4.63	8.00	42.86
<i>Post-treatment (2019Q2-2022Q4)</i>							
Inflow Index	24.74	13.60	2.34	15.33	23.91	31.31	136.07
Outflow Index	18.00	13.44	0.56	9.15	14.54	24.93	113.98
Net Migration	6.75	8.87	-37.75	3.41	5.84	10.51	82.21
Spillover Cities							
<i>Pre-treatment (2018Q2-2019Q1)</i>							
Inflow Index	85.34	65.97	4.43	45.05	63.16	104.54	465.34
Outflow Index	85.83	68.80	3.03	41.54	62.26	106.31	387.31
Net Migration	-0.48	23.24	-150.31	-7.24	1.37	9.45	137.74
<i>Post-treatment (2019Q2-2022Q4)</i>							
Inflow Index	139.91	106.45	1.85	75.30	107.76	165.68	722.15
Outflow Index	139.20	104.75	0.56	72.03	108.22	171.38	670.36
Net Migration	0.71	28.67	-200.04	-11.55	0.86	12.91	196.57
N (Treatment)	60 (pre), 342 (post)						
N (Spillover)	330 (pre), 1881 (post)						

Notes: Treatment cities: Baoshan, Puer, Lincang, Dehong, Nujiang, and Xishuangbanna.